Scale invariance, hysteresis and avalanches in imbibement and drainage

Author: Antonio Turmo Tomás*
Advisor: Jordi Ortín Rull
Facultat de Física, Universitat de Barcelona, / Martí i Franqués 1, 08028 Barcelona, Spain.

Abstract: An exercise of numerical simulation of a quasi-static oil-air displacement through a porous medium is made. The porous medium is modelized through a Hele-Shaw cell and imbibement (wetting), draining (drying) two-phase displacements are studied. It is shown that the displacements present hysteresis and cycle memory. Moreover, it is shown that the oil front movement presents avalanches whose relative frequency is inversely proportional to their size.

I. INTRODUCTION

Characteristics of the motion of two-phase fluids through porous and fractured media are of significant importance to understand the large-scale behaviour of natural and industrial processes such as soil irrigation, carbon sequestration, or secondary oil recovery among others.

These processes have been empirically investigated by studying the motion of sample fluids through Hele-Shaw cells featuring disordered roughness on one side, to replicate for instance the porous nature of open fractures. To be precise, in this work the implementation of the Hele-Shaw cell consists of two flat parallel square plates, with a small separation between them, slightly tilted on one side and inside which a random pattern of gap-thickness contractions-expansions is built. Fig 1 provides a detail of a lateral cut, perpendicular to the fluid movement front. The position of the front at two different moments is shown. The process of advancing the front and therefore increasing the wet surface is called imbibement or imbibition, while the opposite process is called drainage.

The observed behaviour, not yet well understood, has been modelized [1,2] and found it to be dependent on fluid viscosity, surface tension, size and dispersion (disorder) of the rugosities (defects) as well as on hydrostatic pressure and effective gravity (related to the steepness of the cell).

It has been experimentally ascertained that the interphase motion presents hysteresis and return-point memory properties, as well as being characterized by a no smooth motion pattern. The front shows local jumps or avalanches (Haines jumps [1]) of different magnitude and duration.

The motion of the front has been modelized through a quasi-static approach. An equilibrium position of the front is altered by increasing or decreasing the hydrostatic pressure by a tiny finite amount, and then the next equilibrium position of the front is determined.

The purpose of this work is to replicate these phenomena through the implementation of a numerical model of the evolution of the front, when applying increases/decreases in hydrostatic pressure, and to study the properties of the resulting imbibement/drainage front displacements.

II. PHYSICAL SYSTEM, MODEL AND NUMERICAL IMPLEMENTATION

The environment to be modelized is the displacement of a fluid inside a Hele-Shaw cell with a rough side. The fluid moves up and down the cell under the influence of an externally applied hydrostatic pressure, the capillary forces at the interphases and gravity. A scheme can be seen in Fig. 1.

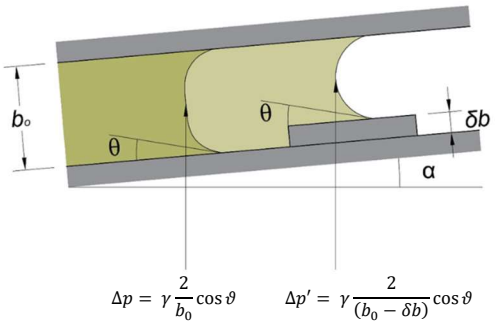

FIG. 1 : Draft of the advancing interphase front. b_0 is the cell height; δb the defect height; α the cell tilting angle, and θ the interface front contact angle with the cell wall.

The motion of the front is simulated by making finite variations of the hydrostatic pressure and then finding the new front equilibrium position, which should fulfil the pressure balance differential equation (for details see [2]):

$$0 = \gamma \frac{\partial^2 h}{\partial x^2} - \rho g_e h(x) + 2\gamma cos\vartheta \frac{\delta b}{{b_0}^2} + \rho g H \qquad (1)$$

where γ means surface tension; h(x), distance to the cell base; x, lateral coordinate; ρ, density of the oil; g, gravity; $g_e = g\, sin\vartheta$, effective gravity; and ρgH the effective hydrostatic pressure, defined as

$$\rho g H = \rho g H' - \gamma \frac{2}{b_0} \cos\vartheta \qquad (2)$$

where ρgH' is the real hydrostatic pressure.

The simulation algorithm works as follows: A front is discretized in so many x points as defined pixels in the width of the cell (see Fig.6). To each point two coordinates are assigned (x, h(x)). To evolve from one equilibrium front to another the hydrostatic pressure is increased/decreased. This increase is determined by dividing the physical height of the whole cell by the number of pixels (height = cell length times $sin\alpha$). Then, for each point of the front, the balance equation (1) is evaluated and if the result differs from zero by more than a given tolerance (1/3000 Pa in the present implementation) a small increase/decrease in h(x) is made. The process is iterated until all the points in the front are inside tolerance. The discrete increase/decrease in h(x) depends on the size of the pixel, effective gravity, density, viscosity and tolerance, following the recommendations to assure algorithm convergence given in [2].

* Electronic address: aturmoto7@alumnes.ub.edu

The implementation has been realized for an oil-air system of $\gamma = 20.7$ mN/m and $\rho = 998$ kg/m³, inside a cell of $b_o = 0.45$ mm; with defects of height $\delta b = 0.06 \pm 0.02$ mm (Gaussian distribution), 0.8 x 0.8 mm of size, covering 35% of the cell surface. The second fluid is considered to be air. As a simplification the contact angle ϑ has been set to zero (perfectly wetting oil), so that $cos\vartheta$ in (1) equals unity.

III. RESULTS: HYSTERESIS CICLE

The results measured as relative fraction of cell wet surface vs applied hydrostatic pressure in Pa for several cell tilt angles can be seen in Fig 2. Solid lines correspond to the imbibement path and dotted lines to the drainage one. The hysteresis phenomena can be clearly appreciated. As it was to be expected, the larger the cell tilt angle, the larger the pressure to be applied in order to get the same percentage of wet surface.

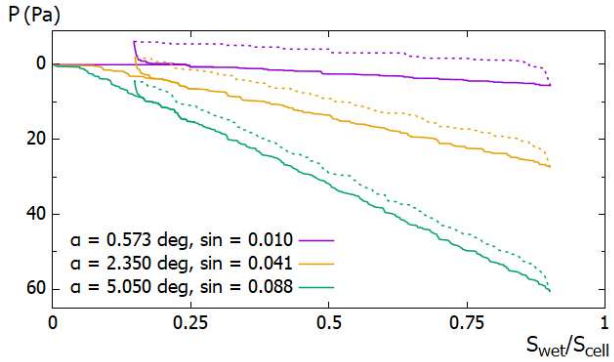

FIG. 2 : Hysteresis cycle for several tilting cell angles. All cell sizes are 80x80 mm, 400x400 pixels.

In Fig 3, the outcome of modelling successive partial imbibement/drainage cycles is depicted. The result of the exercise shows that the cycle has path memory. Although the imbibement/drainage paths are different, for a given disorder realization they are fixed. There is one path for imbibement and another for drainage. Whenever the variation in the hydrostatic pressure is reversed and as a result the front movement changes direction, the front moves to the proper predetermined path.

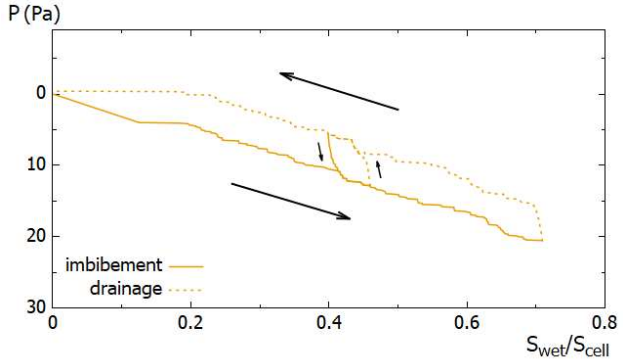

FIG. 3 : Imbibement and drainage processes showing an internal loop with path memory. Cell size 80x80 mm, 400x400 pixel. Tilting angle is 2.350 degrees

The effect of changing the height of the defects without dispersion (disorder of the height) for a given cell size is shown in Fig. 4. Not surprisingly the width of the cycle (dissipated energy) increases with the defect height.

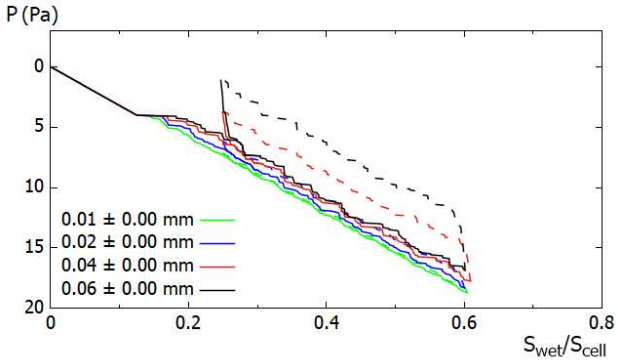

FIG. 4 : Hysteresis cycles for a 80x80 mm, 400x400 pixel cell, with defects of height (0.01, 0.02, 0.04 and 0.06) ± 0.00 mm. Tilting angle of 2.350 degrees.

The effect of variation of the standard deviation of the defect heights for a given cell size and defect mean height is shown in Fig. 5. It is found that the width of the cycles increases with the disorder. This result is in agreement with corresponding results in [2]. Disorder is to be understood here as the spread of the magnitude of the constrictions and expansions (defects) in the cell.

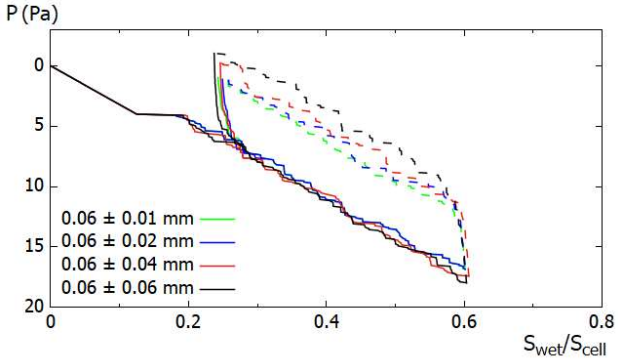

FIG. 5 : Hysteresis cycles for a 80x80 mm, 400x400 pixel cell, with defects of height 0.06 ± (0.01, 0.02, 0.04 and 0.06) mm. Tilting angle of 2.350 degrees.

IV. RESULTS: AVALANCHE SIZE DISTRIBUTION AND FINITE SIZE EFFECTS

Experimental evidence shows that the advance or retreat of a front is not uniform along the line. Rather it presents local jumps of capillary origin, that is to say related to the presence of cell constrictions and expansions (defects). The second derivative in Eq. (1) introduces correlations between individual jumps at adjacent sites, giving rise to Haines jumps, i.e. large and cooperative front displacements between consecutive equilibrium configurations.

In the simulation local avalanches are understood to be local jumps between two consecutive equilibrium positions of one front. An example of avalanche is given in Fig. 6.

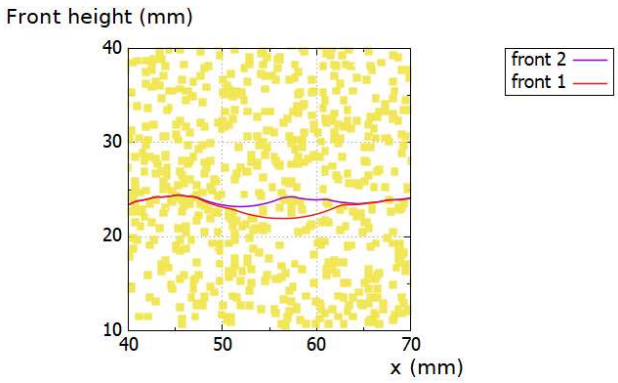

FIG. 6: Detail of a jump between two consecutive front configurations in equilibrium. Cell size 80x80 mm. Defect size 0.8x0.8 mm. Tilting angle of 2.350 degrees.

Avalanches are characterized by their area (size) and their relative frequency. That is to say, the number of occurrences of avalanches of the given size divided by the total number of observed avalanches. The model shows that the smaller the area the larger the frequency, and moreover, that for large ones there is a large dispersion of areas presenting the same low frequency. This can be appreciated in Fig 7 for cells of different sizes but with the same general defect patterns (0.8 x 0.8 mm, $\delta b = 0.06 \pm 0.02$ mm, 35 % cell coverage).

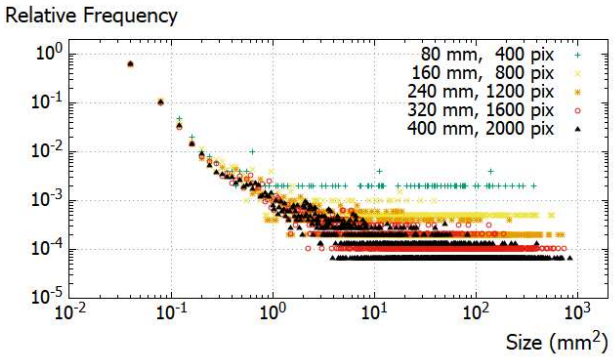

FIG. 7: Relative **f**requency of avalanches vs avalanche size for several cell sizes. Tilting angle of 0.573 degrees.

In order to investigate the dependency of avalanche frequency with avalanche size the large dispersion for large avalanches is a nuisance. To overcome this a move into the continuum is taken, in which a histogram is built such that the width of the bins are increased in a geometrical proportion, so that in a log scale all the class marks are placed at the same intervals, and the frequencies are turned into probability distribution functions (Pdf's), assuring the normalization:

$$\sum_i Ps_i \cdot binwidth_i = 1 \qquad (3)$$

The result is presented in Fig. 8. To facilitate the understanding of the picture, the histograms are not shown, only the class marks.

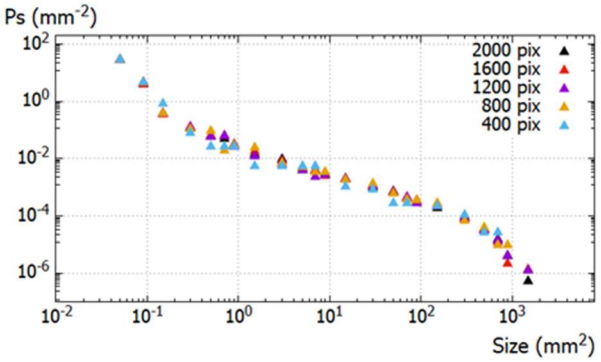

FIG. 8: Probability distribution function vs avalanche size, for different cell sizes. Tilting angle of 0.573 degrees.

The previous chart suggests the existence of two power-law relations between the Pdf and the size of the avalanches, one for very small-sized avalanches and another for medium-sized ones.

The proper way of collapsing the data obtained under different conditions for this kind of phenomena has been discussed by A. Corral [4]. In the case of a power-law behaviour for the intermediate avalanche sizes it should be possible to identify a relation between the variables like

$$P_s(s) \cdot \langle s \rangle^{\frac{m}{2-m}} = A_s \cdot G_s\left(s/s_c\right) \cdot A_s^{\frac{m}{2-m}} \cdot \left(s/s_c\right)^{-m} \qquad (4)$$

where A_s and s_c are constants, being s_c a characteristic cut-off size, such as cell maximum wet surface.

The expected form of G_s suggests that:

$$G_s\left(s/s_c\right) = \phi\left(\, s/\langle s \rangle^{\frac{1}{2-m}} \,\right) \qquad (5)$$

$$P_s(s) \cdot \langle s \rangle^{\frac{m}{2-m}} = \psi\left(\, s/\langle s \rangle^{\frac{1}{2-m}} \,\right) \qquad (6)$$

$$P_s(s) \cdot s^m = As \cdot G_s\left(s/s_c\right) \qquad (7)$$

Defining the first-moment ($\langle s \rangle$) rescaled variables:

$$Y = P_s(s) \cdot \langle s \rangle^{\frac{m}{2-m}}; \quad X = s/\langle s \rangle^{\frac{1}{2-m}} \qquad (8)$$

the exponent m that best collapses the data is found by fitting to the rescaled variables the function

$$Y_{fit} = A.X^{-m}.\exp\left(X/B\right) \qquad (9)$$

for a number of possible "m's" The fitting is limited to avalanches from 0.2 to 150 mm² in size. For each fit the deviation to the real data is computed as

$$\varepsilon(m) = \sum_i \left[\log(Y_i) - \log\left(Y_{fit}\right)\right]^2 \qquad (10)$$

and the one which presents the best adjustment is selected (see Fig. 9). In this way we obtain that m = 1.004. Once the best exponent is determined, the rescaling (8) with the proper exponent is realized and the new variables are represented in Fig. 9, where the collapse is quite evident.

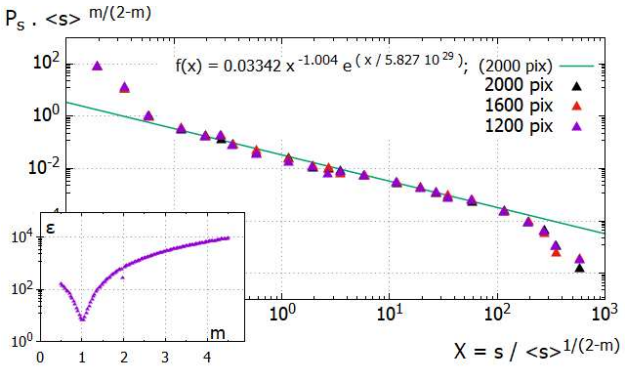

FIG. 9: Collapse of first-moments-normalized Pdf and Size, in the central region of the distribution, from avalanche size 0.2 to 150 mm². The small graph displays the quadratic deviation of the data from the fit as a function of the fitting exponent m. Tilting angle of 0.573 degrees.

The relation (7) is shown in Fig 10, where it can be seen that along the fitting interval $G_s(s/s_c)$ remains constant.

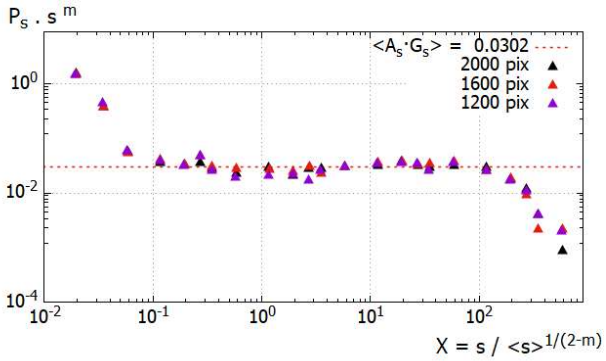

FIG. 10: Graphic representation of $P(s) \cdot s^m$ vs $s/\langle s \rangle^{\frac{1}{2-m}}$, showing the scaling function $G_s(s/s_c)$. Tilting angle of 0.573 degrees.

Following Corral's paper [4] for the steepest part of the Pdf representation, corresponding to avalanche sizes from 0 to 0.2 mm², the following second moment ($\langle s^2 \rangle$) rescaling is realized:

$$Y = P_s(s) \cdot \langle s^2 \rangle^{\frac{m}{3-m}}; \quad X = s/\langle s^2 \rangle^{\frac{1}{3-m}} \qquad (11)$$

In order to find the exponent for the power law a fitting process analogous to the one already carried out for the first moment approach is implemented, producing the result m = 3.693. The collapse of the rescaled variables together with the fitting curve is shown in Fig. 11.

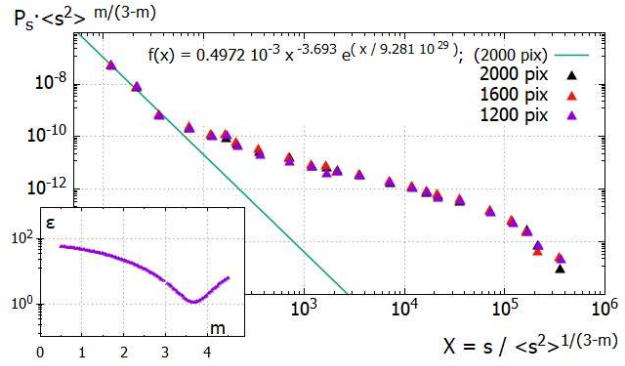

FIG. 11: Collapse of second-moments-normalized Pdf and Size, in the region of the distribution from avalanche size 0 to 0.2 mm^2 The small graph displays the quadratic deviation of the data from the fit as a function of the fitting exponent m. Tilting angle of 0.573 degrees.

V. RESULTS: EFFECTIVE GRAVITY AND AVALANCHE SIZE DISTRIBUTIONS

In this section the effect on the frequency of avalanche sizes of the effective gravity is investigated. The variations of effective gravity are simulated by changing the tilting angle of the cell.

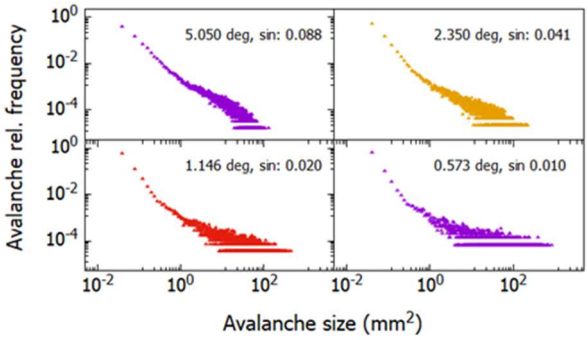

FIG. 12: Frequency of avalanches vs cell tilting angle. Cell size 400x400 mm, 2000x2000 pixels.

As it can be seen the dispersion of the large-sized avalanches decreases with effective gravity. Furthermore, an evolution from a convex to a concave form is appreciated, as a lower effective gravity allows avalanches of larger size.

VI. DISCUSSION AND CONCLUSIONS

The simulations carried out have properly reproduced the pressure vs saturation hysteresis cycle of the imbibement-draining sequence for all cell sizes.

It has also been shown that the hysteresis cycle presents return-point memory. Whenever a cycle is interrupted and reversed it always returns to the same path.

Evidence has been provided that the area and therefore the cycle dissipated energy increases both with the mean height and height dispersion of defects.

The phenomena of avalanches have been set forth, and it has been ascertained that smaller avalanches appear much more frequently than larger ones. A power-law dependence has been investigated, and it has come out that there seems to be two acting laws, one for the tiny avalanches and another for the larger ones. One possible explanation for this could be that small avalanches involve single or small island of defects while large avalanches involve several islands of defects or very large isolated islands. Some insight is given in Fig. 6.

It also seems that the probability distribution function for the avalanche size is rather insensitive to the cell size, even though for the smaller cells the avalanche size pdf is distorted by finite-size effects. One reason for this somewhat poor performance could be the lack of enough statistics. Although the distribution of defects and defect heights has been realized at random, lack of enough computer power has prevented the simulation of more than one configuration for each cell size/defect pattern, while in regular simulations thousands of them would have been needed to get good enough statistics.

Last, effective gravity has been shown to influence the distributions of avalanche sizes, which tend to diverge as effective gravity, or equivalently tilting cell angle, tends to

zero. This behaviour was to be expected since at zero angle the dominant force is the surface tension which is not counteracted by any other one. From the point of view of nonequilibrium critical phenomena the control parameter of the process is effective gravity, and criticality is achieved at zero value, for which the correlation between adjacent sites of the fluid front induced by the in-plane-capillary force has diverging length.

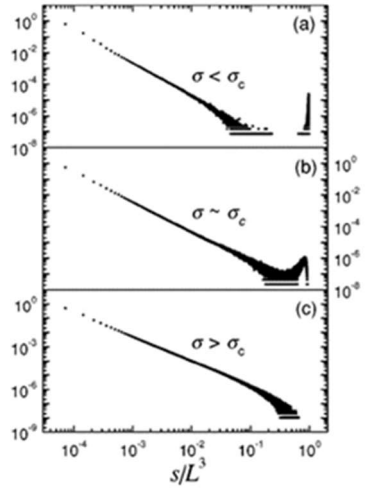

FIG. 13: Reproduction of Fig. 1 from F.J. Pérez Reche and E. Vives [3]. Vertical coordinate shows relative frequency of the avalanches. σ is the control parameter, in this case the standard deviation of the gaussian disorder distribution.

The form and evolution of the avalanches shown in Fig 12 strongly resemble the ones depicted by Pérez-Reche and Vives [3]. In our case the control parameter is the cell tilting angle. It is clearly appreciated the evolution from concave to convex profile while criticality is approached. Criticality in our exercise is achieved when α becomes zero. At this point avalanche sizes are unbounded. Therefore, all the avalanche profiles shown in Figure 12 are subcritical. In our experiment of drainage-imbibement, supercriticality is excluded because the front becomes unstable against viscous fingering during draining.

VII. APPENDIX

Computational environment

Hardware:
Laptop: HP Pavillion G6
Intel Core i3-2350M, 2.30 GHz, 2 cores, 4 threads.
8 GB RAM, 300 GB internal hard disk, 1TB external USB connected hard disk.

Software:
Windows 10 Home
GNU Fortran 5.3.0
GNU Plot 5.2

Processing time to run the simulation for a 2000x2000 pixels cell: one run up to 90% wet surface, 25.5 hours

Acknowledgments

I want to express my gratefulness to my advisor Prof. Jordi Ortín by his unfailing enlightening and exactness, without which this work would have not reached harbour.

I also thank Prof. Francesc Salvat for providing me with an efficient fitting routine based in the symplex method, apt for nonlinear functions, which has dramatically helped me with the fitting section.

I should not forget either to show my gratitude to Profs. Eduard Vives, Carmen Miguel, and all the others who in Collective Phenomena Practices showed me how to tackle this kind of simulations.

And last but not least, my family, who stoically have suffered my confinement inside the confinement, while I have been devoting endless hours to coding, debugging and testing, forgiving me for not paying them the attention that they undoubtedly deserved.

[1] Ramón Planet, Lautaro Díaz-Piola and Jordi Ortín. Capillary jumps of fluid-fluid fronts across an elementary constriction in a model open fracture. Phys. Rev. Fluids **5**, 044002 (2020). DOI: 10.1103/PhysRevFluids.5.044002

[2] Ran Holtzman, Marco Dentz, Ramón Planet and Jordi Ortín. Hysteresis of two-phase flows in disordered media: From micro-scale Haines jumps to macro-scale pressure-saturation curves. Submitted (2020).

[3] Francisco J. Pérez-Reche and Eduard Vives. Finite-size scaling analysis of the avalanches in the three-dimensional Gasussian random-field Ising model with metastable dynamics. Phys.Rev. B **67**, 134421 (2003). DOI : 10.1103/PhysRevB.67.134421

[4] A. Corral. Scaling in the timing of extreme events. Chaos, Solitons & Fractals **74**, 99-112 (2015). DOI: 10.1016/j.chaos.2015.01.011

[5] Kim Christensen and Nicholas R. Moloney. Complexity and Criticality, London; Imperial College Press (2005)

[6] Notes of Computational Physics, Physics Faculty, Universitat de Barcelona (2016).